

Observation of the Borromean three-body Förster resonances for three interacting Rb Rydberg atoms

D. B. Tretyakov^{1,2}, I. I. Beterov^{1,2}, E. A. Yakshina^{1,2}, V. M. Entin^{1,2}, I. I. Ryabtsev^{1,2,*}, P. Cheinet³, and P. Pillet³

¹*Rzhanov Institute of Semiconductor Physics SB RAS, 630090 Novosibirsk, Russia*

²*Novosibirsk State University, 630090 Novosibirsk, Russia and*

³*Laboratoire Aimé Cotton, CNRS, Univ. Paris-Sud, ENS Paris-Saclay, 91405 Orsay, France*

(Dated: 6 July 2017)

Three-body Förster resonances at long-range interactions of Rydberg atoms were first predicted and observed in Cs Rydberg atoms by R.Faoro et al., *Nature Comm.* **6**, 8173 (2015). In these resonances, one of the atoms carries away an energy excess preventing the two-body resonance, leading thus to a Borromean type of Förster energy transfer. But they were in fact observed as the average signal for the large number of atoms $N \gg 1$. In this Letter we report on the first experimental observation of the three-body Förster resonances $3 \times nP_{3/2}(|M|) \rightarrow nS_{1/2} + (n+1)S_{1/2} + nP_{3/2}(|M^*|)$ in a few Rb Rydberg atoms with $n = 36, 37$. We have found here clear evidence that there is no signature of the three-body Förster resonance for exactly two interacting Rydberg atoms, while it is present for $N=3-5$ atoms. This demonstrates the assumption that three-body resonances can generalize to any Rydberg atom. As such resonance represents an effective three-body operator, it can be used to directly control the three-body interactions in quantum simulations and quantum information processing with Rydberg atoms.

PACS numbers: 32.80.Ee, 32.70.Jz, 32.80.Rm, 03.67.Lx

Highly excited Rydberg atoms exhibit strong long-range interactions due to their huge dipole moments that grow as n^2 with increasing the principal quantum number n [1]. This is especially attractive for the development of quantum computers and simulators based on qubits represented by single alkali-metal atoms in the arrays of optical dipole traps or optical lattices [2-5]. In particular, Rydberg-atom-based quantum simulators can directly model various objects in solid-state physics due to their ability to mimic various possible interactions between their constituents, if such interactions in a quantum simulator are appropriately controlled [6-14].

Interactions between Rydberg atoms are flexibly controlled by the dc or radiofrequency (rf) electric field via Stark-tuned [15], microwave [16-19] or rf-assisted [4,16] Förster resonances corresponding to the Förster resonant energy transfer (FRET). Förster resonances have been demonstrated to be efficient tools in cold Rydberg atoms [20, 21] to tune interactions in strength and distance and can be either resonant dipole-dipole or nonresonant van der Waals interactions. The interactions are typically described by a two-body operator of dipole-dipole interaction for each pair of atoms in the ensemble [1]. After such interaction the two atoms are found in an entangled state, so that a measurement over one atom deterministically predicts the state of the other atom. This entanglement is the quantum resource, which is used in quantum computations and simulations [2-13,22].

Some exotic quantum simulations demand to control the interactions of simultaneously three atoms [22-28]. This demands a three-body quantum operator that

changes the states of the three qubits simultaneously and makes them all entangled. Three-body operators are described by a combination of two-body operators, which in fact are reduced to a single effective three-body operator.

Such operator has been proposed and implemented recently as a Borromean three-body FRET in a frozen Rydberg gas of Cs atoms [29]. In these three-body resonances, one of the atoms carries away an energy excess preventing the two-body resonance, leading thus to a Borromean type of Förster energy transfer. Here the Borromean transfer is featured by the strong isolated three-body energy transfer with a negligible contribution of two-body effect. This allows to characterize the three-body effect while it is usually impossible in other systems because it is imbedded in the strong two-body effect signal. The experiment in Ref. [29] was done with an ensemble of $\sim 10^5$ Cs atoms in the interaction volume of $\sim 200 \mu\text{m}$ in size. Therefore, the three-body Förster resonance was in fact observed as the average signal for the large number of atoms $N \gg 1$.

In this Letter we present the first experimental observation of the Borromean three-body Förster resonance $3 \times nP_{3/2}(|M|) \rightarrow nS_{1/2} + (n+1)S_{1/2} + nP_{3/2}(|M^*|)$ for $N=3-5$ Rb Rydberg atoms with $n = 36, 37$. We have found clear evidence that there is no signature of the three-body Förster resonances for exactly two interacting Rydberg atoms, while it is present for the larger number of atoms. We thus demonstrate the possible generalization of this effect to other Rydberg atoms.

The experiments are performed with cold ^{85}Rb atoms in a magneto-optical trap [4,30]. Our experiments feature atom-number-resolved measurement of the signals obtained from $N=1-5$ detected Rydberg atoms with a detection efficiency of $\approx 70\%$ [31]. It is based on a selective field ionization (SFI) detector with channel electron

*Electronic address: ryabtsev@isp.nsc.ru

multiplier (CEM) and post-selection technique [32]. The CEM output pulses from the nS and $[nP+(n+1)S]$ states (the two latter states have nearly identical ionizing fields and are detected together) are detected with two independent gates and post-selected over the number of the detected Rydberg atoms $N=1-5$. The normalized N -atom signals S_N are the fractions of atoms that have undergone a transition to the final nS state. We can record Förster resonances for up to five detected Rydberg atoms and compare these with theory.

In this experiment the detection of N Rydberg atoms means that there were N interacting Rydberg atoms with $\approx 70\%$ confidence and $N+1$ interacting atoms with $\approx 30\%$ confidence. Therefoere, the recorded Förster resonance spectra were additionally processed to extract the true multi-atom spectra ρ_i taking into account finite detection efficiency (Supplementary Material, Section 1).

The excitation of Rb atoms to the $nP_{3/2}$ Rydberg states is realized via three-photon transition $5S_{1/2} \rightarrow 5P_{3/2} \rightarrow 6S_{1/2} \rightarrow nP_{3/2}$ by means of three cw lasers modulated to form 2 μ s exciting pulses at a repetition rate of 5 kHz [4,33]. Small Rydberg excitation volume of $\sim 15 \mu\text{m}$ in size is formed using the crossed tightly-focused laser beams. The laser intensities are adjusted to obtain about one Rydberg atom excited per laser pulse on average. We use a Stark-switching technique [33,34] to switch the Rydberg interactions on and off. Laser excitation occurs during 2 μ s at a fixed electric field of 5.6 V/cm. Then the field decreases to a lower value near the resonant electric field, which acts for 3 μ s until the field increases back to 5.6 V/cm. Then, 0.5 μ s later, a ramp of the strong field-ionizing electric pulse of 200 V/cm is applied. The lower electric field is slowly scanned across the Förster resonance and the SFI signals are accumulated for $10^3 - 10^4$ laser pulses.

Figure 1 presents the numerically calculated Stark structure of the Förster resonance $3 \times 37P_{3/2} \rightarrow 37S_{1/2} + 38S_{1/2} + 37P_{3/2}^*$ for three Rb Rydberg atoms. The energies W of various three-body collective states are shown versus the controlling dc electric field. The intersections between collective states (labeled by numbers) correspond to the Förster resonances of various kinds. The intersections 2-7 are in fact two-body resonances that do not require the third atom. The intersections 1 and 8 are three-body resonances occurring only in the presence of the third atom that carries away an energy excess preventing the two-body resonance.

The intersections 2-7 are in fact two-body resonances that do not require the third atom and can be observed for two atoms. In such resonances, the dipole-dipole interaction induces transitions from the initial $37P_{3/2}$ state to the final $37S_{1/2}$ and $38S_{1/2}$ states in two of the three atoms, while the third atom remains in its initial P state that does not change.

The intersections 1 and 8 are three-body resonances occurring only in the presence of the third atom that carries away an energy excess preventing the two-body resonance, leading thus to a Borromean type of Förster energy transfer [29]. The three-body resonances are distinguished from the two-body ones by the fact that the third atom does not remain in its initial P state as its initial moment projection ($|M|=1/2$ or $|M|=3/2$) changes to the other one ($|M^*|=3/2$ or $|M^*|=1/2$, correspondingly).

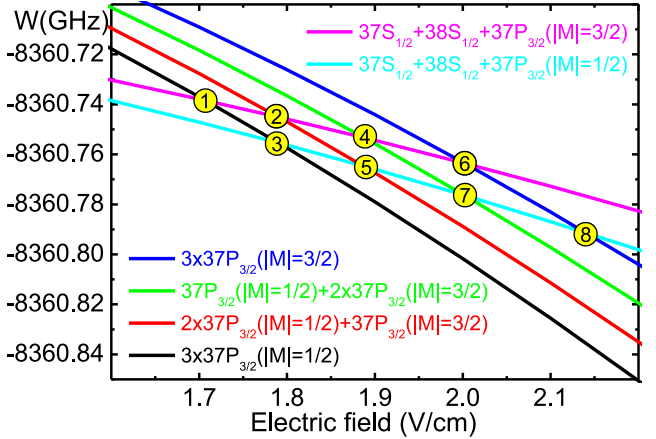


FIG. 1: (color online) Numerically calculated Stark structure of the Förster resonance $3 \times 37P_{3/2} \rightarrow 37S_{1/2} + 38S_{1/2} + 37P_{3/2}^*$ for three Rb Rydberg atoms. The energies W of various three-body collective states are shown versus the controlling electric field. The intersections between collective states (labeled by numbers) correspond to the Förster resonances of various kinds. The intersections 2-7 are in fact two-body resonances that do not require the third atom. The intersections 1 and 8 are three-body resonances occurring only in the presence of the third atom that carries away an energy excess preventing the two-body resonance.

Therefore, the three-body resonance corresponds to the transition when the three interacting atoms change their states simultaneously.

In our experiments, cold Rb atoms are excited in the dc electric field either to the initial $37P_{3/2}(|M|=1/2)$ Stark sublevel or to the $37P_{3/2}(|M|=3/2)$ one. Therefore, not all resonances 1-8 in Fig. 1 can be observed simultaneously. For the initial state $37P_{3/2}(|M|=1/2)$ only the resonances 1 and 3 are observable, while for the initial state $37P_{3/2}(|M|=3/2)$ we can only observe the resonances 6 and 8. The intermediate resonances 2, 4, 5 and 7 are observable only when both $|M|=1/2$ and $|M|=3/2$ atoms are initially excited, as in our earlier paper [35] where we used the excitation by broadband pulsed lasers.

Figures 2(a) and 2(b) show the Stark-tuned Förster resonances observed for various numbers of the interacting atoms $i=2-5$. The recorded resonances S_N have been additionally processed to extract the true multi-atom resonances ρ_i taking into account finite detection efficiency (Supplementary Material, Section 1). In Fig. 2(a) the atoms are in the initial state $37P_{3/2}(|M|=1/2)$. The main peak at 1.79 V/cm is the ordinary two-body resonance that occurs for all $i=2-5$ and corresponds to the intersection 3 in Fig. 1. This resonance was studied in detail in our previous papers [31,33]. The additional peak at 1.71 V/cm is the predicted three-body resonance 1 of Fig. 1 that is absent for $i=2$ and appears only for $i=3-5$. The two-body and three-body peak positions well agree with those predicted by Fig. 1.

The feature at 1.71 V/cm could in principle be caused by the imperfection of the electric-field pulses used to

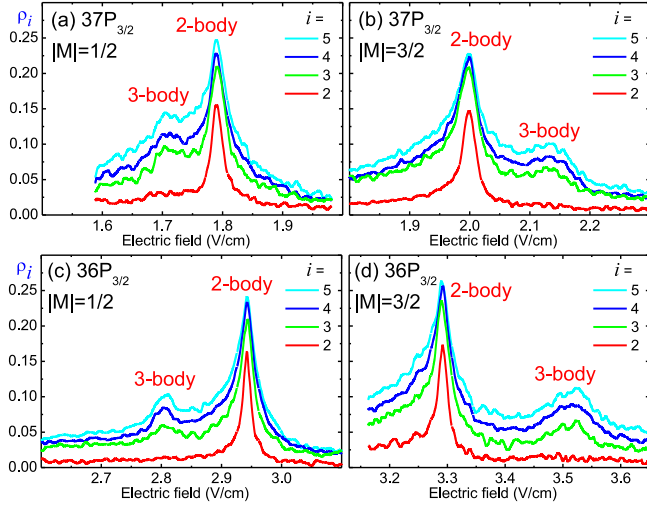


FIG. 2: (color online) Stark-tuned Förster resonances in Rb Rydberg atoms observed for various numbers of atoms $i=2-5$ and various initial states: (a) $37P_{3/2}(|M|=1/2)$; (b) $37P_{3/2}(|M|=3/2)$; (c) $36P_{3/2}(|M|=1/2)$; (d) $36P_{3/2}(|M|=3/2)$. The main peaks are two-body resonances, the additional peaks are three-body resonances. The three-body resonance is absent for $i=2$ in all records, evidencing its three-body nature.

control the Förster resonance, as it was observed and discussed in our paper [33]. In order to check for this effect, the resonance has also been recorded for atoms in the initial state $37P_{3/2}(|M|=3/2)$, as shown in Fig. 1(b). We see that the three-body resonance changes its position with respect to the two-body resonance, in full agreement with Fig. 1. Again, the main peak at 2.0 V/cm is the ordinary two-body resonance that occurs for all $i=2-5$. The additional peak at 2.14 V/cm is the three-body resonance that is absent for $i=2$ and appears only for $i=3-5$. We conclude that the three-body resonances really take place, as their positions and behavior well agree with theoretical predictions. The imperfection of the electric-field pulses results only in the slight asymmetry of the main two-body resonances.

Figures 2(a) and 2(b) show that the two-body and three-body resonances partially overlap. This overlapping increases as i grows due to the increase of the total interaction energy and broadening of the two-body resonance. The overlapping can be reduced if a lower Rydberg state is used [29]. For example, if we take atoms in the initial state $36P_{3/2}$, the Stark structure of the Förster resonance is the same as in Fig. 1, but the separation between intersections 1 and 3 is 140 mV/cm instead of 80 mV/cm for the $37P_{3/2}$ atoms. Figures 2(c) and 2(d) present the two-body and three-body resonances recorded for atoms in the initial state $36P_{3/2}$. The resonances are similar to those in Figs. 2(a) and 2(b), but are better visible due to the larger separation. They additionally confirm that the three-body resonances really take place and can be observed separately from the two-

body ones.

In our previous experiments [31,33], we used only atoms in the initial state $37P_{3/2}(|M|=1/2)$. Therefore, in the related theoretical analysis [31,33,36] we considered only the two-body resonance 3 of Fig. 1 and ignored the possibility of the three-body resonance 1. As a result, the numerically calculated multi-atom spectra ρ_i for $i=2-5$ were not disturbed by the three-body resonance and had symmetric line shapes. Our present experiment has revealed that the three-body resonance affects the line shapes for $i=3-5$ and causes the asymmetry. This asymmetry indicates that some atoms undergo a nonresonant transition from the initial state $37P_{3/2}(|M|=1/2)$ to another Stark sublevel $37P_{3/2}(|M^*|=3/2)$, but such transition is not described by the two-body operator of dipole-dipole interaction. This requires a new theoretical model to be developed. It is rather complicated problem since we should take into account all Stark and magnetic sublevels of the interacting Rydberg atoms. In this paper we limited our theoretical considerations only by the cases of two and three interacting Rydberg atoms.

For two Rydberg atoms in the initial state $37P_{3/2}(|M|=1/2)$ only one Förster resonance 3 of Fig. 1 is possible, which corresponds to the resonant transition between two collective states $2 \times 37P_{3/2}(|M|=1/2) \rightarrow 37S_{1/2} + 38S_{1/2}$. Its dipole-dipole matrix element is given by

$$V = \frac{d_1 d_2}{4\pi\epsilon_0} \left[\frac{1}{R^3} - \frac{3Z^2}{R^5} \right], \quad (1)$$

where d_1, d_2 are the z components of the matrix elements of dipole moments of transitions $|37P_{3/2}(M=1/2)\rangle \rightarrow |37S_{1/2}(M=1/2)\rangle$ and $|37P_{3/2}(M=1/2)\rangle \rightarrow |38S_{1/2}(M=1/2)\rangle$, Z is the z component of the vector \mathbf{R} connecting the two atoms (z axis is chosen along the dc electric field), and ϵ_0 is the dielectric constant. For the weak interaction, the two-body Förster resonance amplitude is $\rho_2 \sim V^2$ [26].

For three Rydberg atoms in the initial state $37P_{3/2}(|M|=1/2)$ the two Förster resonances 1 and 3 of Fig. 1 are possible. The three-body resonance 1 corresponds to the resonant transition between collective states $3 \times 37P_{3/2}(|M|=1/2) \rightarrow 37S_{1/2} + 38S_{1/2} + 37P_{3/2}(|M^*|=3/2)$. This transition is in fact composed of the two non-resonant two-body relay transitions $3 \times 37P_{3/2}(|M|=1/2) \rightarrow 37S_{1/2} + 38S_{1/2} + 37P_{3/2}(|M|=1/2) \rightarrow 37S_{1/2} + 38S_{1/2} + 37P_{3/2}(|M^*|=3/2)$ occurring simultaneously. The latter occurs due to non-resonant exchange interaction $nP_{3/2}(M) + n'S \rightarrow n'S + nP_{3/2}(M^*)$ corresponding to the excitation hopping between S and P Rydberg atoms [29,36]. Despite the use of a relay, the transfer occurs in a single step, implying a Borromean character of the relay atom which absorbs the energy of the finite Förster defect. The perturbation theory (Supplementary Material, Section 2) shows that for the weak interaction the three-body Förster resonance amplitude is

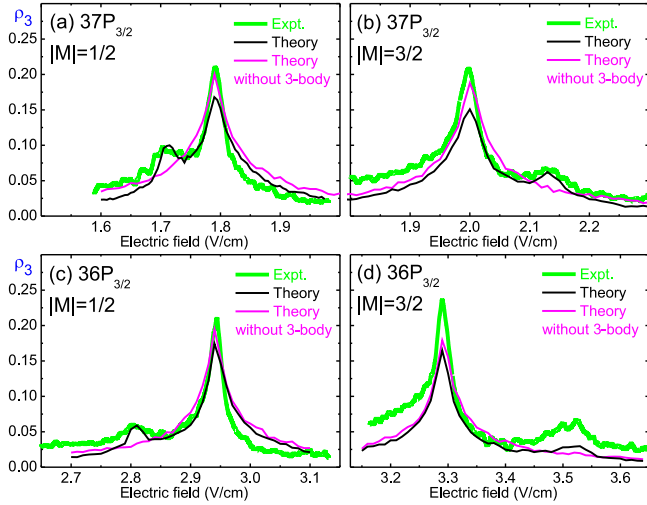


FIG. 3: (color online) Comparison between theory and experiment for the three-atom Stark-tuned Förster resonances $3 \times 3P_{3/2}(|M|) \rightarrow nS_{1/2} + (n+1)S_{1/2} + nP_{3/2}(|M^*|)$ in Rb Rydberg atoms for the initial states: (a) $37P_{3/2}(|M|=1/2)$; (b) $37P_{3/2}(|M|=3/2)$; (c) $36P_{3/2}(|M|=1/2)$; (d) $36P_{3/2}(|M|=3/2)$. The theoretical spectra have been calculated for the cubic interaction volume of $15 \times 15 \times 15 \mu\text{m}^3$, $3 \mu\text{s}$ interaction time and Monte Carlo averaging over 1000 random atom positions. The thick green (grey) lines are experiment, the thin black lines are full theory, and the thin magenta (dark grey) lines are theory without accounting for the three-body resonances.

$\rho_3 \sim (VV^*/\Delta)^2$, where V^* is the same as V but for the transitions $|37P_{3/2}(M=3/2)\rangle \rightarrow |37S_{1/2}(M=1/2)\rangle$ and $|37P_{3/2}(M=3/2)\rangle \rightarrow |38S_{1/2}(M=1/2)\rangle$, and $\Delta/(2\pi)=9.5$ MHz is the energy splitting between $37P_{3/2}(|M|=1/2)$ and $37P_{3/2}(|M|=3/2)$ Stark sublevels in the electric field of 1.71 V/cm.

The three-body resonance is thus less effective than the two-body one at the weak dipole-dipole interaction ($V < \Delta$). However, when the three-body resonance is exactly tuned, its contribution to the population transfer generally exceeds the contribution from two-body interaction, which is off-resonant in this case (Supplementary Material, Section 2). The condition for the three-body resonance to be of the Borromean type is thus satisfied.

We have done numerical simulations of the experimental Förster resonances of Fig. 2 for $i=3$ atoms using the method described in Refs. [31,36]. It is based upon solving the Schrödinger's equation with subsequent Monte Carlo averaging over the random positions of the three atoms in a single interaction volume (Supplementary Material, Section 3). The Stark and Zeeman structures of all Rydberg states are fully taken into account. The numerical results and their comparison with the experimental data of Fig. 2 are presented in Fig. 3. The thick green (grey) lines are the experimental three-atom data, the thin black lines are full theory, and the thin magenta (dark grey) lines are theory without accounting for the three-body resonances. The theoretical spectra have

been calculated and averaged over 1000 random atom positions for the cubic interaction volume of $15 \times 15 \times 15 \mu\text{m}^3$ and $3 \mu\text{s}$ interaction time, which correspond to our experimental parameters.

The overall agreement of the full theory with experiment in Fig. 3 is satisfactory. The calculated line shapes of the two-body resonances are close to the experimental ones. These are cusp-shaped resonances that are formed upon spatial averaging in a single interaction volume, as discussed in our paper [33] and other papers [37,38]. When the three-body resonances are not accounted for by theory, the height of the two-body peak grows because the population does not leak to the other three-atom states, while the three-body peaks are absent at all. The three-body resonances are well reproduced by theory in Figs. 3(a)-3(c), both in their heights and widths. However, some discrepancy between experiment and theory is found for the $36P_{3/2}(|M|=3/2)$ state atoms in Fig. 3(d). The theory predicts weaker two- and three-body Förster resonances than those observed experimentally. One of the explanations could be a smaller laser excitation volume in this particular experiment compared to the other ones, but numerical simulations have shown that smaller volume results in the poorer agreement for the two-body resonance. This discrepancy points towards the need to build a new model based on the density-matrix equations, as we did for $i=2$ atoms in Ref. [33], but this is a complicated task which requires a dedicated study.

To conclude, our experiments with a few Rb Rydberg atoms in various initial states have clearly shown the need for three atoms to obtain a three-body resonance signature in perfect agreement with expectations. The three-body resonance corresponds to a transition when the three interacting atoms change their states simultaneously (two atoms go to the S states and the third one remains in the P state but changes its moment projection). Such Borromean-type transfer displays strong three-body energy transfer with a negligible contribution of two-body transfer. As the three-body resonance appears at the different dc electric field with respect to the two-body resonance, it represents an effective three-body operator, which can be used to directly control the three-body interactions. This can be especially useful in quantum simulations and quantum information processing with neutral atoms in optical lattices [2-15]. It can also allow to test and study a quantum system where the basic interaction is a three-body interaction.

We note that the Borromean trimers of Rydberg atoms have been predicted in Ref. [39] and excitation transfer in a spin chain of three Rydberg atoms has been observed experimentally in Ref. [40]. We also note that in principle it is possible to organize three-body interactions for almost arbitrary Rydberg states using the radiofrequency-assisted Förster resonances occurring between Floquet sidebands of Rydberg states in a radiofrequency electric field [41]. Finally, Förster resonances of the higher orders (four-body etc.) can also be observed in the electric field which is different from the two-body one [29,42].

The authors are grateful to Elena Kuznetsova and Mark Saffman for fruitful discussions. This work was supported by the RFBR Grants No. 16-02-00383 and 17-02-00987, the Russian Science Foundation Grant No. 16-12-00028 (for laser excitation of Rydberg states), the

Siberian Branch of RAS, the Novosibirsk State University, the public Grant CYRAQS from Labex PALM (ANR-10-LABX-0039) and the EU H2020 FET Proactive project RySQ (Grant No. 640378).

[1] T. F. Gallagher, *Rydberg Atoms* (Cambridge University Press, Cambridge, 1994).

[2] M. Saffman, T. G. Walker, and K. Mølmer, Quantum information with Rydberg atoms, *Rev. Mod. Phys.* **82**, 2313 (2010).

[3] D. Comparat and P. Pillet, Dipole blockade in a cold Rydberg atomic sample, *J. Opt. Soc. Am. B* **27**, A208 (2010).

[4] I. I. Ryabtsev, I. I. Beterov, D. B. Tretyakov, V. M. Entin, and E. A. Yakshina, Spectroscopy of cold rubidium Rydberg atoms for applications in quantum information, *Physics - Uspekhi* **59**, 196 (2016).

[5] M. Saffman, Quantum computing with atomic qubits and Rydberg interactions: progress and challenges, *J. Phys. B* **49**, 202 (2016).

[6] H. Weimer, M. Müller, I. Lesanovsky, P. Zoller, and H. P. Büchler, A Rydberg quantum simulator, *Nature Phys.* **6**, 382 (2010).

[7] J. P. Hague and C. MacCormick, Quantum simulation of electron-phonon interactions in strongly deformable materials, *New J. Phys.* **14**, 033019 (2012).

[8] A. Dauphin, M. Müller, and M. A. Martin-Delgado, Rydberg-atom quantum simulation and Chern-number characterization of a topological Mott insulator, *Phys. Rev. A* **86**, 053618 (2012).

[9] J. P. Hague and C. MacCormick, Bilayers of Rydberg Atoms as a Quantum Simulator for Unconventional Superconductors, *Phys. Rev. Lett.* **109**, 223001 (2012).

[10] A. W. Glatzle, M. Dalmonte, R. Nath, I. Rousochatzakis, R. Moessner, and P. Zoller, Quantum Spin-Ice and Dimer Models with Rydberg Atoms, *Phys. Rev. X* **4**, 041037 (2014).

[11] M. Mattioli, A. W. Glatzle, and W. Lechner, From classical to quantum non-equilibrium dynamics of Rydberg excitations in optical lattices, *New J. Phys.* **17**, 113039 (2015).

[12] J. Gelhausen, M. Buchhold, A. Rosch, and P. Strack, Quantum-optical magnets with competing short- and long-range interactions: Rydberg-dressed spin lattice in an optical cavity, *SciPost Phys.* **1**(1), 004 (2016).

[13] A. Dauphin, M. Müller, and M. A. Martin-Delgado, Quantum simulation of a topological Mott insulator with Rydberg atoms in a Lieb lattice, *Phys. Rev. A* **93**, 043611 (2016).

[14] W. Maineult, B. Pelle, R. Faoro, E. Arimondo, P. Pillet, and P. Cheinet, Dipole-quadrupole Förster resonance in cesium Rydberg gas, *J. Phys B* **49**, 214001 (2016).

[15] K. A. Safinya, J. F. Delpech, F. Gounand, W. Sandner, and T. F. Gallagher, Resonant Rydberg-atom – Rydberg-atom collisions, *Phys. Rev. Lett.* **47**, 405 (1981).

[16] P. Pillet, D. Comparat, M. Muldrich, T. Vogt, N. Zazham, V. M. Akulin, T. F. Gallagher, W. Li, P. Tanner, M. W. Noel, and I. Mourachko, Coherence and decoherence in Rydberg gases, in *Decoherence, Entanglement and Information Protection in Complex Quantum Systems*, edited by V. M. Akulin and G. Kurizki (Springer, New York, 2005).

[17] P. Pillet, R. Kachru, N. H. Tran, W. W. Smith, and T. F. Gallagher, Radiative collisions in strong field regime, *Phys. Rev. Lett.* **50**, 1763 (1983).

[18] P. Pillet, R. Kachru, N. H. Tran, W. W. Smith, and T. F. Gallagher, Radiative Rydberg atom – Rydberg atom collisions in the strong field regime, *Phys. Rev. A* **36**, 1132 (1987).

[19] J. Lee and T. F. Gallagher, Microwave transitions from pairs of $Rb\,nd_{5/2}nd_{5/2}$ atoms, *Phys. Rev. A* **93**, 062509 (2016).

[20] W. R. Anderson, J. R. Veale, and T. F. Gallagher, Resonant dipole-dipole energy transfer in a nearly frozen Rydberg gas, *Phys. Rev. Lett.* **80**, 249 (1998).

[21] I. Mourachko, D. Comparat, F. de Tomasi, A. Fioretti, P. Nosbaum, V. M. Akulin, and P. Pillet, Many-body effects in a frozen Rydberg gas, *Phys. Rev. Lett.* **80**, 253 (1998).

[22] I. M. Georgescu, S. Ashhab, and F. Nori, Quantum simulation, *Rev. Mod. Phys.* **86**, 153 (2014).

[23] H.-W. Hammer, A. Nogga, and A. Schwenk, Three-body forces: From cold atoms to nuclei, *Rev. Mod. Phys.* **85**, 197 (2013).

[24] W. Liu, J. Zhang, Z. Deng, and G. Long, Simulation of general three-body interactions in a nuclear magnetic resonance ensemble quantum computer, *Sci. China Ser. G* **51**, 1089 (2008).

[25] X. Peng, J. Zhang, J. Du, and D. Suter, Quantum simulation of a system with competing two- and three-body interactions, *Phys. Rev. Lett.* **103**, 140501 (2009).

[26] K. Jachymski, P. Bienias, and H. P. Büchler, Three-body interaction of Rydberg slow light polaritons, *Phys. Rev. Lett.* **117**, 053601 (2016).

[27] W. L. You, Y. C. Qiu, and A. M. Oles, Quantum phase transitions in a generalized compass chain with three-site interactions, *Phys. Rev. B* **93**, 214417 (2016).

[28] Z. Luo, C. Lei, J. Li, X. Nie, Z. Li, X. Peng, and J. Du, Experimental observation of topological transitions in interacting multispin systems, *Phys. Rev. A* **93**, 052116 (2016).

[29] R. Faoro, B. Pelle, A. Zuliani, P. Cheinet, E. Arimondo, and P. Pillet, Borromean three-body FRET in frozen Rydberg gases, *Nature Comm.* **6**, 8173 (2015).

[30] D. B. Tretyakov, I. I. Beterov, V. M. Entin, I. I. Ryabtsev, and P. L. Chapovsky, Investigation of cold rubidium Rydberg atoms in a magneto-optical trap, *J. Exper. Theor. Phys.* **108**, 374 (2009).

[31] I. I. Ryabtsev, D. B. Tretyakov, I. I. Beterov, and V. M. Entin, Observation of the Stark-tuned Förster resonance between two Rydberg atoms, *Phys. Rev. Lett.* **104**, 073003 (2010).

[32] I. I. Ryabtsev, D. B. Tretyakov, I. I. Beterov, and

V. M. Entin, Effect of finite detection efficiency on the observation of the dipole-dipole interaction of a few Rydberg atoms, *Phys. Rev. A* **76**, 012722 (2007); Erratum: *Phys. Rev. A* **76**, 049902(E) (2007).

[33] E. A. Yakshina, D. B. Tretyakov, I. I. Beterov, V. M. Entin, C. Andreeva, A. Cinins, A. Markovski, Z. Iftikhar, A. Ekers, and I. I. Ryabtsev, Line shapes and time dynamics of the Förster resonances between two Rydberg atoms in a time-varying electric field, *Phys. Rev. A* **94**, 043417 (2016).

[34] I. I. Ryabtsev, D. B. Tretyakov, and I. I. Beterov, Stark-switching technique for fast quantum gates in Rydberg atoms, *J. Phys. B* **36**, 297 (2003).

[35] D. B. Tretyakov, I. I. Beterov, V. M. Entin, E. A. Yakshina, I. I. Ryabtsev, S. F. Dyubko, E. A. Alekseev, N. L. Pogrebnyak, N. N. Bezuglov, and E. Arimondo, Effect of photoions on the line Shape of the Förster resonance lines and microwave transitions in cold rubidium Rydberg atoms, *J. Exper. Theor. Phys.* **114**, 14 (2012).

[36] I. I. Ryabtsev, D. B. Tretyakov, I. I. Beterov, V. M. Entin, and E. A. Yakshina, Stark-tuned Förster resonance and dipole blockade for two to five cold Rydberg atoms: Monte-Carlo simulations for various spatial configurations, *Phys. Rev. A* **82**, 053409 (2010).

[37] B. G. Richards and R. R. Jones, Dipole-dipole resonance line shapes in a cold Rydberg gas, *Phys. Rev. A* **93**, 042505 (2016).

[38] H. Park, T. F. Gallagher, and P. Pillet, Microwave pump-probe spectroscopy of the dipole-dipole interaction in a cold Rydberg gas, *Phys. Rev. A* **93**, 052501 (2016).

[39] M. Kiffner, W. Li, and D. Jaksch, Three-Body Bound States in Dipole-Dipole Interacting Rydberg Atoms, *Phys. Rev. Lett.* **111**, 233003 (2013).

[40] D. Barredo, H. Labuhn, S. Ravets, T. Lahaye, A. Browaeys, and C. S. Adams, Coherent Excitation Transfer in a Spin Chain of Three Rydberg Atoms, *Phys. Rev. Lett.* **114**, 113002 (2015).

[41] D. B. Tretyakov, V. M. Entin, E. A. Yakshina, I. I. Beterov, C. Andreeva, and I. I. Ryabtsev, Controlling the interactions of a few cold Rb Rydberg atoms by radio-frequency-assisted Förster resonances, *Phys. Rev. A* **90**, 041403(R) (2014).

[42] J. H. Gurian, P. Cheinet, P. Huillery, A. Fiorette, J. Zhao, P. L. Gould, D. Comparat, and P. Pillet, Observation of a Resonant Four-Body Interaction in Cold Cesium Rydberg Atoms, *Phys. Rev. Lett.* **108**, 023005 (2012).

Appendix: SUPPLEMENTARY MATERIAL

1. Derivation of the true many-body spectra from the experimental multiatom spectra of the Förster resonances

The measured normalized N -atom signals S_N are the fractions of atoms that have undergone a transition to the final nS state (or the population of the nS state per atom). As shown in our paper [S1], for the non-ideal selective-field-ionization (SFI) detector, which detects fewer atoms than actually have interacted, various true multiatom spectra ρ_i of the Förster resonances for i interacting Rydberg atoms contribute to our measured

signals S_N for N detected Rydberg atoms to a degree that depends on the mean number of the detected atoms. The signals S_N are thus a mixture of the spectra ρ_i from the larger numbers of actually interacted atoms $i \geq N$:

$$S_N = \rho + e^{-\bar{n}(1-T)} \sum_{i=N}^{\infty} \rho_i \frac{[\bar{n}(1-T)]^{i-N}}{(i-N)!}, \quad (\text{A.1})$$

where ρ is a nonresonant background signal due to blackbody-radiation-induced transitions and background collisions, \bar{n} is the mean number of Rydberg atoms excited per laser pulse, and T is the detection efficiency of the SFI detector. The value of ρ should be the same for various N since it is caused by the parasitic transitions in each single atom.

The mean number of detected Rydberg atoms is $\bar{n}T$. The measurement of this value and of the relationship

$$\alpha = (S_1 - \rho) / (S_2 - \rho) \quad (\text{A.2})$$

at zero Förster detuning can provide a measurement of the unknown values of \bar{n} and T . In Ref. [S1] we considered the case of the weak dipole-dipole interaction, when the following scaling was assumed to be valid:

$$\rho_i \approx (i-1) \rho_2, \quad (\text{A.3})$$

For this case it was shown that

$$\bar{n} \approx [\alpha / (1 - \alpha) + \bar{n}T]. \quad (\text{A.4})$$

This expression, however, is valid only for the very weak dipole-dipole interaction, when multiatom Förster resonances are far below the saturation, as it was in our experiment with the Na thermal atomic beam [S1].

Now let us consider an example of the multiatom Förster resonance for $36P_{3/2}(|M| = 1/2)$ atoms recorded for the interaction time of $3 \mu\text{s}$ in our present experiment, shown in Fig. 4(a). Our aim is to make a decomposition of the experimental records $S_1 - S_5$ for $N=1-5$ detected Rydberg atoms in order to obtain the true multiatom spectra ρ_i of the Förster resonances for exactly i interacting Rydberg atoms, which are defined according to Eq. (A.1). For this purpose, we first need to find the unknown values of \bar{n} and T .

As a starting point, for this experiment we already know the mean number of the detected Rydberg atoms $\bar{n}T \approx 1.05$, which was specially measured and recorded in each experiment. Then, using Eq. (A.4) we in principle can find \bar{n} and T . However, Eq. (A.4) seems to be invalid for Fig. 4(a), because the spectra are close to the saturation and Eq. (A.3) obviously does not work. Therefore we need first to modify Eq. (A.4) for the case of saturation.

Figure 5(a) presents the results of numerical simulations for the theoretical multiatom two-body spectra ρ_i

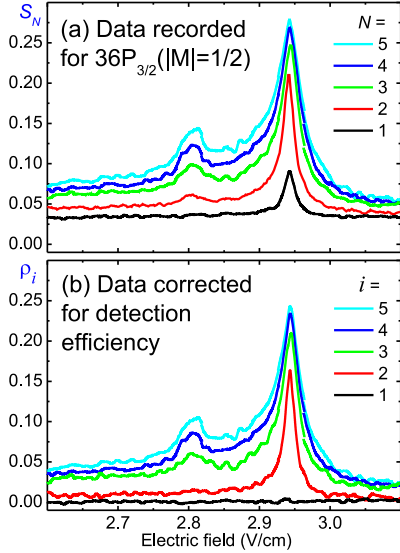


FIG. 4: (color online) (a) Raw data S_N recorded for the Stark-tuned Förster resonance in Rb Rydberg atoms for various numbers of the detected atoms $N=1-5$ and initial state $36P_{3/2}(|M|=1/2)$. Presence of the resonance for $N=1$ is due to the finite detection efficiency of 72%. (b) True multiatom spectra ρ_i derived from S_N . The data are corrected for the detection efficiency using the procedure described in the text.

for the $36P_{3/2}(|M|=1/2)$ atoms in the cubic interaction volume of $17 \times 17 \times 17 \mu\text{m}^3$ for the interaction time of $3 \mu\text{s}$ (these parameters are close to the experimental ones). It is seen that at zero detuning the amplitudes of all resonances saturate at the 0.25 value. Therefore, at zero detuning instead of Eq. (A.3) we should now adopt that $\rho_2 \approx \rho_3 \approx \rho_4 \approx \rho_5 \approx \dots$. Then Eqs. (A.1) and (A.2) give

$$\alpha \approx 1 - e^{-\bar{n}(1-T)}, \quad (\text{A.5})$$

$$\bar{n} \approx \ln \frac{1}{1 - \alpha} + \bar{n}T. \quad (\text{A.6})$$

The values of $\rho \approx 0.029$, $S_1=0.09$ and $S_2=0.21$ have been measured from the spectra in Fig. 4(a). This allows us to find $\alpha \approx 0.34$, $\bar{n} \approx 1.46$, and $T \approx 0.72$. With these values we can explicitly write down the expansion coefficients for the multiatom spectra in Eq. (A.1):

$$\begin{aligned} S_1 &= \rho + 0.66\rho_1 + 0.27\rho_2 + 0.06\rho_3 + 0.01\rho_4 + \dots, \\ S_2 &= \rho + 0.66\rho_2 + 0.27\rho_3 + 0.06\rho_4 + 0.01\rho_5 + \dots, \\ S_3 &= \rho + 0.66\rho_3 + 0.27\rho_4 + 0.06\rho_5 + 0.01\rho_6 + \dots, \\ S_4 &= \rho + 0.66\rho_4 + 0.27\rho_5 + 0.06\rho_6 + 0.01\rho_7 + \dots, \\ S_5 &= \rho + 0.66\rho_5 + 0.27\rho_6 + 0.06\rho_7 + 0.01\rho_8 + \dots. \end{aligned} \quad (\text{A.7})$$

In Eqs. (A.7) we should take into account that $\rho_1 = 0$ in S_1 , because there is no interaction for a single atom.

In order to derive ρ_2 and ρ_3 , which are necessary for the analysis of the three-body Förster resonance, we should

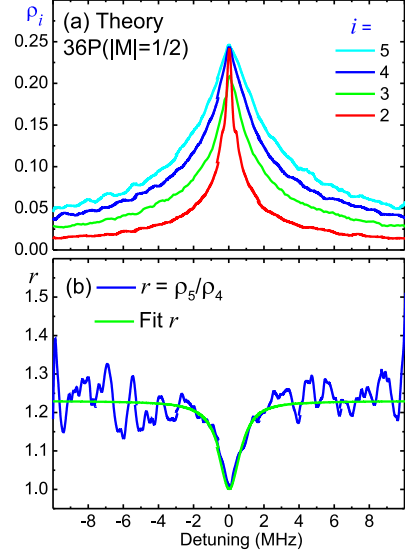


FIG. 5: (color online) (a) Numerical simulation of the two-body Förster resonance in Rb Rydberg atoms for various numbers of the interacting atoms $i=2-5$ in the initial state $36P_{3/2}(|M|=1/2)$. The theoretical spectra have been calculated with the Schrödinger's equation for the cubic interaction volume of $17 \times 17 \times 17 \mu\text{m}^3$, $3 \mu\text{s}$ interaction time and Monte Carlo averaging over 1000 random atom positions. (b) Ratio of the spectra ρ_5 and ρ_4 is shown by the blue (dark grey) curve, and its fit by the inverted Lorentz function is shown by the green (light grey) curve.

simplify Eqs. (A.7) to exclude the terms with large numbers of atoms. First, the terms with the weight of 0.01 have small contribution and with a small error can be just added to the preceding terms as follows:

$$\begin{aligned} S_1 &= \rho + 0.27\rho_2 + 0.07\rho_3, \\ S_2 &= \rho + 0.66\rho_2 + 0.27\rho_3 + 0.07\rho_4, \\ S_3 &= \rho + 0.66\rho_3 + 0.22\rho_4 + 0.07\rho_5, \\ S_4 &= \rho + 0.66\rho_4 + 0.27\rho_5 + 0.07\rho_6, \\ S_5 &= \rho + 0.66\rho_5 + 0.27\rho_6 + 0.07\rho_7. \end{aligned} \quad (\text{A.8})$$

Second, we believe that the multiatom spectra in Fig. 4(a) are reliably measured for $N=1-4$, while the spectrum for $N=5$ can be affected by the nonlinearity of our channeltron. Therefore, in the further analysis we will consider only the experimental spectra with $N=1-4$ and need to exclude ρ_5 and ρ_6 in Eqs. (A.8). This can be done if we approximately express ρ_5 and ρ_6 via ρ_4 using the theoretical curves in Fig. 5(a). Figure 5(b) shows as the blue (dark grey) curve the ratio $r = \rho_5/\rho_4$ taken from Fig. 5(a). This ratio depends on the detuning: it is 1 at zero detuning due to saturation and 1.23 at large detunings. The fluctuations of r at large detunings in Fig. 5(b) are due to insufficient statistics of the averaging of small signals, which can be smoothed if the statistics increases or using the fitting function. We have found a fitting function for this dependence [green (grey) curve in Fig. 5(b)]:

$$r(\Delta) \approx 1.23 - 0.23 \frac{0.5}{0.5 + \Delta^2}, \quad (\text{A.9})$$

where detuning Δ is defined by the electric field F (V/cm) for the $36P_{3/2}(|M|=1/2)$ atoms as

$$\Delta(\text{MHz}) = -229.73 + 2.93F + 25.494F^2. \quad (\text{A.10})$$

In the further analysis we take $\rho_5 \approx \rho_4 r(\Delta)$. We can also adopt with some precision that $\rho_6 \approx \rho_5 r(\Delta) \approx \rho_4 r^2(\Delta)$ in Eqs. (A.8), although we did not calculate ρ_6 directly.

With the above assumptions Eqs. (A.8) are modified as

$$\begin{aligned} S_1 &= \rho + 0.27\rho_2 + 0.07\rho_3, \\ S_2 &= \rho + 0.66\rho_2 + 0.27\rho_3 + 0.07\rho_4, \\ S_3 &= \rho + 0.66\rho_3 + [0.27 + 0.07r(\Delta)]\rho_4, \\ S_4 &= \rho + [0.66 + 0.27r(\Delta) + 0.07r^2(\Delta)]\rho_4. \end{aligned} \quad (\text{A.11})$$

The straightforward calculations with Eqs. (A.11) give us the true multi-atom spectra $\rho_2 - \rho_4$ expressed via the measured value of ρ and spectra $S_2 - S_4$ of Fig. 4(a):

$$\begin{aligned} \rho_4 &\approx \frac{S_4 - \rho}{0.66 + 0.27r(\Delta) + 0.07r^2(\Delta)}, \\ \rho_3 &\approx \frac{S_3 - \rho}{0.66} - [0.41 + 0.1r(\Delta)]\rho_4, \\ \rho_2 &\approx \frac{S_2 - \rho}{0.66} - 0.41\rho_3 - 0.1\rho_4. \end{aligned} \quad (\text{A.12})$$

In order to derive Eqs. (A.12) we used only the equations for $S_2 - S_4$ in Eqs. (A.11). But after calculating ρ_2 and ρ_3 with Eqs. (A.12) we should also check for the identity

$$\rho_1 \approx (S_1 - \rho - 0.272\rho_2 - 0.064\rho_3)/0.66 \approx 0, \quad (\text{A.13})$$

which means that we correctly decomposed the measured spectra $S_2 - S_4$ into true multiautom spectra.

Figure 5(b) presents the true multiautom spectra ρ_i derived from Fig. 5(a) with Eqs. (A.12). The black curve for ρ_1 represents the identity of Eq. (A.13). We see that in the 2-atom spectrum the feature at 1.71 V/cm has disappeared, while in the 3-atom spectrum it is still present. It indicates that in this experiment we really observe the Borromean three-body resonance. The validity of the above considerations is confirmed by the fact that the identity of Eq. (A.13) is well satisfied in Fig. 4(b), being nearly zero.

The other experimental records (Fig. 2 of the main paper) have been processed in the same way as the records in Fig. 4. We note that the approach we have used here is similar to the approach we applied earlier to decompose the selective-field-ionization signals from four-body resonances in Cs Rydberg atoms [S2].

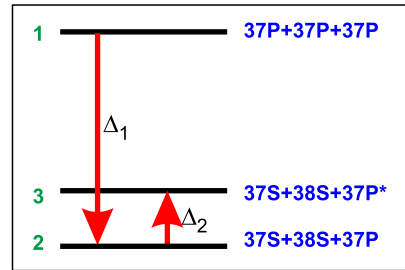


FIG. 6: (color online) Simplified scheme of the three-body Förster resonance $3 \times nP_{3/2}(|M|=1/2) \rightarrow nS_{1/2} + (n+1)S_{1/2} + nP_{3/2}^* (|M|=3/2)$ for three Rydberg atoms. The initially populated collective state 1 is $3 \times nP_{3/2}(|M|=1/2)$. The final collective state 3 is $nS_{1/2} + (n+1)S_{1/2} + nP_{3/2}^* (|M|=3/2)$ with the changed moment projection of the P state. The intermediate collective state 2 is $nS_{1/2} + (n+1)S_{1/2} + nP_{3/2} (|M|=1/2)$ with the initial moment projection of the P state. The energy defects Δ_1 and Δ_2 are controlled by the dc electric field. The value of Δ_1 can be arbitrary, while Δ_2 is nonzero and nearly constant in the vicinity of the Förster resonance. The three-body resonance occurs at $\Delta_1 = \Delta_2$, while the two-body one occurs at $\Delta_1 = 0$.

2. Analytical model for a Borromean three-body Förster resonance

Figure 6 shows a simplified scheme of the Borromean three-body Förster resonance $3 \times nP_{3/2}(|M|=1/2) \rightarrow nS_{1/2} + (n+1)S_{1/2} + nP_{3/2}^* (|M|=3/2)$ for three interacting Rydberg atoms. The initially populated collective state 1 is $3 \times nP_{3/2}(|M|=1/2)$. The final collective state 3 is $nS_{1/2} + (n+1)S_{1/2} + nP_{3/2}^* (|M|=3/2)$ with the changed moment projection of the P state. The intermediate collective state 2 is $nS_{1/2} + (n+1)S_{1/2} + nP_{3/2} (|M|=1/2)$ with the initial moment projection of the P state. The energy defects Δ_1 and Δ_2 are controlled by the dc electric field. The value of Δ_1 can be arbitrary, while Δ_2 is nonzero and nearly constant in the vicinity of the Förster resonance. The three-body resonance occurs at $\Delta_1 = \Delta_2$, while the two-body one occurs at $\Delta_1 = 0$.

For the simplicity, we consider a triangle spatial configuration of the three frozen Rydberg atoms spaced by the equal distances R . The dipole-dipole matrix element for the two-body transition 1 \rightarrow 2 is given by

$$V = \frac{d_1 d_2}{4\pi\epsilon_0} \left[\frac{1}{R^3} - \frac{3Z^2}{R^5} \right], \quad (\text{A.14})$$

where d_1, d_2 are the z components of the matrix elements of dipole moments of transitions $|nP_{3/2} (M=1/2)\rangle \rightarrow |nS_{1/2} (M=1/2)\rangle$ and $|nP_{3/2} (M=1/2)\rangle \rightarrow |(n+1)S_{1/2} (M=1/2)\rangle$, Z is the z component of the vector connecting the two atoms \mathbf{R} (z axis is chosen along the dc electric field), and ϵ_0 is the dielectric constant.

The dipole-dipole matrix element V^* for the two-body transition 2 \rightarrow 3 is given by an equation simi-

lar to Eq. (A.14), but for the x and y components of the connecting vector and dipole moments of transitions $|nP_{3/2}(M=3/2)\rangle \rightarrow |nS_{1/2}(M=1/2)\rangle$ and $|nP_{3/2}(M=3/2)\rangle \rightarrow |(n+1)S_{1/2}(M=1/2)\rangle$.

States 2 and 3 are actually six-fold degenerate with respect to the atom permutations. Therefore, there are totally six transitions with the matrix element V from state 1 to state 2 and twelve allowed transitions with the matrix element V^* from state 2 to state 3. The Schrödinger's equation then gives for the probability amplitudes $a_1 - a_3$ of the degenerate sublevels of states 1–3:

$$\begin{aligned} i\dot{a}_1 &= 6\Omega a_2 e^{-i\Delta_1 t}, \\ i\dot{a}_2 &= \Omega a_1 e^{i\Delta_1 t} + 2\Omega^* a_3 e^{i\Delta_2 t}, \\ i\dot{a}_3 &= 2\Omega^* a_2 e^{-i\Delta_2 t}. \end{aligned} \quad (\text{A.15})$$

Here $\Omega = V/\hbar$ and $\Omega^* = V^*/\hbar$. Equations (A.15) can be solved analytically. After several substitutions we come to a single differential equation

$$\begin{aligned} \ddot{a}_3 + i(2\Delta_2 - \Delta_1)\ddot{a}_3 + [\Delta_2(\Delta_1 - \Delta_2) + \\ 4\Omega^{*2} + 6\Omega^2]\dot{a}_3 - 4i(\Delta_1 - \Delta_2)\Omega^{*2} = 0. \end{aligned}$$

Then we seek the solution as $a_3 \sim e^{i\mu t}$ and obtain the cubic equation,

$$\begin{aligned} \mu^3 + (2\Delta_2 - \Delta_1)\mu^2 - [\Delta_2(\Delta_1 - \Delta_2) + \\ 4\Omega^{*2} + 6\Omega^2]\mu + 4(\Delta_1 - \Delta_2)\Omega^{*2} = 0. \end{aligned}$$

This equation has three roots, which are found analytically with the following sequence of equations taken from the mathematical handbooks:

$$\begin{aligned} S &= -[\Delta_2(\Delta_1 - \Delta_2) + 4\Omega^{*2} + 6\Omega^2], \\ T &= 4(\Delta_1 - \Delta_2)\Omega^{*2}, \\ A &= S - (2\Delta_2 - \Delta_1)^2/3, \\ B &= 2(2\Delta_2 - \Delta_1)^3/27 - (2\Delta_2 - \Delta_1)S/3 + T, \\ D &= (A/3)^3 + (B/2)^2, \\ U &= (-B/2 + \sqrt{D})^{1/3}, \\ U^* &= -(B/2 + \sqrt{D})^{1/3}. \end{aligned}$$

Finally, the three roots are

$$\begin{aligned} \mu_1 &= U + U^* - (2\Delta_2 - \Delta_1)/3, \\ \mu_2 &= -(U + U^*)/2 + i\sqrt{3}(U - U^*)/2, \\ \mu_3 &= -(U + U^*)/2 - i\sqrt{3}(U - U^*)/2. \end{aligned}$$

Then we seek a_3 in the form

$$a_3 = c_1 e^{i\mu_1 t} + c_2 e^{i\mu_2 t} + c_3 e^{i\mu_3 t}$$

with the initial conditions $a_3(0) = 0$; $\dot{a}_3(0) = 0$; $\ddot{a}_3(0) = -2\Omega\Omega^*$. These conditions give us the final exact analytical solution for the coefficients,

$$\begin{aligned} c_1 &= \frac{2\Omega\Omega^*}{(\mu_2 - \mu_1)(\mu_1 - \mu_3)}, \\ c_2 &= \frac{2\Omega\Omega^*}{(\mu_2 - \mu_1)(\mu_3 - \mu_2)}, \\ c_3 &= \frac{2\Omega\Omega^*}{(\mu_1 - \mu_3)(\mu_3 - \mu_2)}. \end{aligned}$$

These formulas allow us to find a_3 analytically. Then we can find a_2 using

$$a_2 = i\dot{a}_3 e^{i(\Delta_2 - \Delta_1)t}/(2\Omega^*)$$

and thus find the exact analytical solution to Eqs. (A.15) for arbitrary interaction energy, detunings, and t . Taking into account the six-fold level degeneracy, the three-atom resonance spectrum is then calculated as

$$\rho_3 = (6|a_2|^2 + 6|a_3|^2)/3. \quad (\text{A.16})$$

The exact analytical formulas are rather complex and cannot be presented in a clearly understandable way. Therefore, below we consider the case of the weak dipole-dipole interaction, when most of the population remains in the initial state 1, and final states 2 and 3 are weakly populated. In this case, the approximate analytical solution of Eqs. (A.15) and Eq. (A.16) yields

$$\begin{aligned} \rho_3 \approx \frac{8\Omega^2}{\Delta_1^2} \sin^2 \left[\frac{\Delta_1 t}{2} \right] + 32\Omega^2\Omega^{*2} \times \\ \left\{ \frac{1}{\Delta_1\Delta_2(\Delta_1 - \Delta_2)^2} \sin^2 \left[\frac{(\Delta_1 - \Delta_2)t}{2} \right] + \right. \\ \left. \frac{1}{\Delta_1\Delta_2^2(\Delta_1 - \Delta_2)} \sin^2 \left[\frac{\Delta_2 t}{2} \right] - \right. \\ \left. \frac{1}{\Delta_1^2\Delta_2(\Delta_1 - \Delta_2)} \sin^2 \left[\frac{\Delta_1 t}{2} \right] \right\}. \end{aligned} \quad (\text{A.17})$$

The first term in Eq. (A.17) is responsible for the two-body resonance at $\Delta_1 = 0$. The resonance amplitude grows as $\rho_3 \rightarrow 2\Omega^2 t^2$, while its width is given by the Fourier width of the interaction pulse. Upon spatial averaging, this resonance obtains the cusped line shape, while the Rabi-like population oscillations are washed out, as discussed in our paper [S3].

The third and the fourth terms in Eq. (A.17) do not give any resonance at $\Delta_1 = \Delta_2$ as they compensate for each other with Δ_2 being nonzero and nearly constant in the vicinity of the Förster resonance. At $\Delta_1 = 0$ the fourth term just reduces the first 2-body term, while the second and the third terms compensate for each other as well.

It is the second term in Eq. (A.17) which is responsible for the Borromean three-body resonance at $\Delta_1 = \Delta_2$. Its amplitude grows as $\rho_3 \rightarrow 8\Omega^2\Omega^{*2}t^2/\Delta_2^2$. The relationship between amplitudes of the three-body and two-body resonances is $4\Omega^{*2}/\Delta_2^2$. Therefore, the three-body resonance is always weaker than the two-body resonance for the weak dipole-dipole interaction ($4\Omega^{*2} < \Delta_2^2$). For example, $\Delta_2/(2\pi) = 9.5$ MHz for the $37P_{3/2}(|M|=1/2)$ and $37P_{3/2}(|M|=3/2)$ Stark sublevels of Rb atoms in the electric field of 1.71 V/cm corresponding to the three-body resonance, while the average dipole-dipole interaction energy is below 1 MHz in our experiments.

However, when the three-body resonance is exactly tuned at $\Delta_1 = \Delta_2$, its contribution to the population transfer generally exceeds the contribution from two-body interaction, which is off-resonant in this case. From Eq. (A.17) we find that the three-body contribution relates to the two-body contribution as $2\Omega^{*2}t^2$ and can be large for the long interaction times. This is the main condition for the three-body resonance to be of the Borromean type.

Equation (A.17) helps to understand which parameters are responsible for the two- and three-body Förster resonances. However, it is not valid to describe these resonances at the strong dipole-dipole interaction or long interaction time, since the two-body resonance saturates and broadens [A3]. In this case, only numerical simulations are applicable, as described in the next section. Numerical simulations also provide spatial averaging over the random atom positions and account for the orientation of atomic dipoles, as well as the Stark and Zeeman structures of Rydberg states.

3. Full theory of the dipole-dipole interaction in a three-atom ensemble and numerical simulations

The electric dipole-dipole interaction between two atoms 1 and 2 is described by the operator

$$\hat{V}_{dd} = \frac{1}{4\pi\epsilon_0 R_{12}^3} \left[\hat{\mathbf{d}}_1 \hat{\mathbf{d}}_2 - 3 \left(\hat{\mathbf{d}}_1 \mathbf{n}_{12} \right) \left(\hat{\mathbf{d}}_2 \mathbf{n}_{12} \right) \right]. \quad (\text{A.18})$$

Here R_{12} is the interatomic distance, $\mathbf{n}_{12} = (\cos\varphi\sin\theta, \sin\varphi\sin\theta, \cos\theta)$ is a unit vector in the direction connecting two atoms, and $\hat{\mathbf{d}}_1$ and $\hat{\mathbf{d}}_2$ are dipole-moment operators for these two atoms. By introducing the components of the dipole operators in the spherical basis [S4] for each atom k as $\hat{d}_{k,\pm} = \mp \left(\hat{d}_{k,x} \pm i\hat{d}_{k,y} \right) / \sqrt{2}$, we expand the operator of dipole-dipole interaction as follows:

$$\begin{aligned} \hat{V}_{dd} = & \frac{1}{4\pi\epsilon_0 R_{12}^3} \times \\ & \left[A_1(\theta) \left(\hat{d}_{1+} \hat{d}_{2-} + \hat{d}_{1-} \hat{d}_{2+} + 2\hat{d}_{1z} \hat{d}_{2z} \right) + \right. \\ & A_2(\theta, \varphi) \left(\hat{d}_{1+} \hat{d}_{2z} - \hat{d}_{1-} \hat{d}_{2z} + \hat{d}_{1z} \hat{d}_{2+} - \hat{d}_{1z} \hat{d}_{2-} \right) + \\ & A_3(\theta, \varphi) \left(\hat{d}_{1+} \hat{d}_{2z} + \hat{d}_{1-} \hat{d}_{2z} + \hat{d}_{1z} \hat{d}_{2+} + \hat{d}_{1z} \hat{d}_{2-} \right) + \\ & A_4(\theta, \varphi) \left(\hat{d}_{1+} \hat{d}_{2+} + \hat{d}_{1-} \hat{d}_{2-} \right) + \\ & \left. A_5(\theta, \varphi) \left(\hat{d}_{1+} \hat{d}_{2+} - \hat{d}_{1-} \hat{d}_{2-} \right) \right]. \end{aligned}$$

Here the angular pre-factors are

$$\begin{aligned} A_1(\theta) &= \frac{1 - 3\cos^2(\theta)}{2}, \\ A_2(\theta, \varphi) &= \frac{3\sin(2\theta)\cos(\varphi)}{2\sqrt{2}}, \\ A_3(\theta, \varphi) &= -i\frac{3\sin(2\theta)\sin(\varphi)}{2\sqrt{2}}, \\ A_4(\theta, \varphi) &= -\frac{3\sin^2(\theta)\cos(2\varphi)}{2}, \\ A_5(\theta, \varphi) &= i\frac{3\sin^2(\theta)\sin(2\varphi)}{2}. \end{aligned}$$

The operator \hat{V}_{dd} couples the states where the total magnetic quantum number $m = m_1 + m_2$ changes by $\Delta m = 0, \pm 1, \pm 2$. The matrix element of the \hat{V}_{dd} operator for a transition between the collective two-atom states $|\gamma_a, \gamma_b\rangle \rightarrow |\gamma_s, \gamma_t\rangle$, where for each atomic state $|\gamma\rangle = |nljm_j\rangle$ n is the principal quantum number, l is the orbital moment, j is the total moment and m_j is the projection of the total moment, is expressed as [S5,S6]

$$\begin{aligned}
& \langle n_s m_s l_s j_s; n_t m_t l_t j_t | \hat{V}_{dd} | n_a m_a l_a j_a; n_b m_b l_b j_b \rangle = \\
& = \frac{e^2}{4\pi\epsilon_0 R_{12}^3} \left\{ A_1(\theta) \left[C_{j_a m_a 11}^{j_s m_s} C_{j_b m_b 1-1}^{j_t m_t} + \right. \right. \\
& \left. \left. C_{j_a m_a 1-1}^{j_s m_s} C_{j_b m_b 11}^{j_t m_t} + 2C_{j_a m_a 10}^{j_s m_s} C_{j_b m_b 10}^{j_t m_t} \right] + \right. \\
& A_2(\theta, \varphi) \left[\left(C_{j_a m_a 11}^{j_s m_s} - C_{j_a m_a 1-1}^{j_s m_s} \right) C_{j_b m_b 10}^{j_t m_t} + \right. \\
& \left. C_{j_a m_a 10}^{j_s m_s} \left(C_{j_b m_b 11}^{j_t m_t} - C_{j_b m_b 1-1}^{j_t m_t} \right) \right] + \\
& A_3(\theta, \varphi) \left[\left(C_{j_a m_a 11}^{j_s m_s} + C_{j_a m_a 1-1}^{j_s m_s} \right) C_{j_b m_b 10}^{j_t m_t} + \right. \\
& \left. C_{j_a m_a 10}^{j_s m_s} \left(C_{j_b m_b 11}^{j_t m_t} + C_{j_b m_b 1-1}^{j_t m_t} \right) \right] + \\
& A_4(\theta, \varphi) \left[C_{j_a m_a 11}^{j_s m_s} C_{j_b m_b 11}^{j_t m_t} + C_{j_a m_a 1-1}^{j_s m_s} C_{j_b m_b 1-1}^{j_t m_t} \right] + \\
& A_5(\theta, \varphi) \left[C_{j_a m_a 11}^{j_s m_s} C_{j_b m_b 11}^{j_t m_t} - C_{j_a m_a 1-1}^{j_s m_s} C_{j_b m_b 1-1}^{j_t m_t} \right] \times \\
& \sqrt{\max(l_a, l_s)} \sqrt{\max(l_b, l_t)} \sqrt{(2j_a + 1)(2j_b + 1)} \times \\
& \times \left\{ \begin{array}{ccc} l_a & 1/2 & j_a \\ j_s & 1 & l_s \end{array} \right\} \left\{ \begin{array}{ccc} l_b & 1/2 & j_b \\ j_t & 1 & l_b \end{array} \right\} (-1)^{l_s + \frac{l_a + l_s + 1}{2}} \times \\
& (-1)^{l_t + \frac{l_b + l_t + 1}{2}} (-1)^{j_a + j_b} R_{n_a l_a}^{n_s l_s} R_{n_b l_b}^{n_t l_t}.
\end{aligned}$$

Here $R_{n_a l_a}^{n_s l_s}$ and $R_{n_b l_b}^{n_t l_t}$ are radial matrix elements for $|n_a l_a\rangle \rightarrow |n_s l_s\rangle$ and $|n_b l_b\rangle \rightarrow |n_t l_t\rangle$ transitions, respectively. The radial matrix elements are calculated using the quasiclassical approximation [S7].

In our numerical simulations we consider collective states of the three atoms $|\gamma_1 \gamma_2 \gamma_3\rangle = |n_1 l_1 j_1 m_{j1}; n_2 l_2 j_2 m_{j2}; n_3 l_3 j_3 m_{j3}\rangle$. For example, if the atoms are initially excited to the $37P_{3/2}$ state, we take into account the eight atomic states $|37P_{3/2}, m_j = \pm 1/2\rangle$, $|37P_{3/2}, m_j = \pm 3/2\rangle$, $|37S_{1/2}, m_j = \pm 1/2\rangle$, and $|38S_{1/2}, m_j = \pm 1/2\rangle$. The initial state of the three-atom system is taken as random superposition of the eight degenerate collective states where all three atoms are in the $|37P_{3/2}, m_j = \pm 1/2\rangle$ states (or in the $|37P_{3/2}, m_j = \pm 3/2\rangle$ states, if the exciting laser is tuned to the excitation of the $37P_{3/2}$ atoms with $|m_j| = 3/2$), with equal statistical weights. Here we assume that after laser excitation the sign of $m = m_1 + m_2$ for the initial state is undetermined. The Förster energy defect is the difference between the energies of the final collective state $|\gamma_1 \gamma_2 \gamma_3\rangle$ and of the initial state. To reduce the complexity of the calculations, we do not take into account far-detuned collective states with the Förster energy defect exceeding 2 GHz.

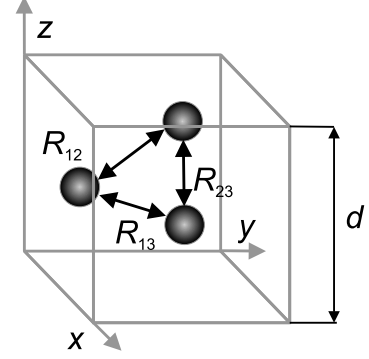


FIG. 7: Geometry of the interaction of the three Rydberg atoms randomly positioned in a cubic volume, used in the numerical simulations with subsequent Monte Carlo averaging over the atom positions.

The same approach is used in the numerical simulations for the initially excited $36P_{3/2}$ atoms, where the eight atomic states $|36P_{3/2}, m_j = \pm 1/2\rangle$, $|36P_{3/2}, m_j = \pm 3/2\rangle$, $|36S_{1/2}, m_j = \pm 1/2\rangle$, and $|37S_{1/2}, m_j = \pm 1/2\rangle$ should be taken into account.

In order to simulate the experimental data, we consider the three atoms, randomly located in a single cubic interaction volume with the edge length d , as shown in Fig. 7. The quantization axis z is chosen along the external electric field. For each random spatial configuration we calculate the interatomic distances R_{12} , R_{23} , R_{13} and the angles θ_{12} , θ_{23} , θ_{13} , φ_{12} , φ_{23} , φ_{13} between the quantization axis and the vectors connecting the atoms.

We calculate the matrix of the Hamiltonian for collective states $|\gamma_1 \gamma_2 \gamma_3\rangle$ of the three-atom system, taking into account the Stark shifts of the atomic energy levels in the external dc electric field as the variation of the diagonal terms of the Hamiltonian and the dipole-dipole interaction of atoms. The numerically calculated polarizabilities of the relevant Rydberg states are listed in Table 1.

Table 1. Calculated polarizabilities of Rydberg states.

State	$ m_j $	α , MHz/(V/cm) 2
$36S_{1/2}$	1/2	5.03
$37S_{1/2}$	1/2	6.11
$38S_{1/2}$	1/2	7.37
$36P_{3/2}$	1/2	31.73
$37P_{3/2}$	1/2	38.9
$36P_{3/2}$	3/2	26.46
$37P_{3/2}$	3/2	32.47

Then we solve numerically the Schrödinger's equation for the probability amplitudes of all collective states for the interaction time $\tau = 3 \mu\text{s}$ used in the experiments. The probability ρ_3 to find one of the atoms in the final $37S$ state for initially excited $37P_{3/2}$ atoms or in the final $36S$ state for initially excited $36P_{3/2}$ atoms is calculated versus the controlling dc electric field. For each

field value we average the calculated probabilities over 1000 random spatial configurations. The results of our numerical simulations are presented in Fig. 3 of the main text. We observe the good qualitative and satisfactory quantitative agreement between theory and experiment. Nevertheless, as some discrepancies are still seen, in our future numerical simulations we plan to use a more complicated density-matrix model [S3], which demands much longer computation time.

We have also compared our numerical simulations with the experiment for two interacting atoms. Only two-body Förster resonance appears both in theory and experiment for each initially excited state, in contrast to three-atom spectra. This confirms that our method of simulating the multiatom signals is valid.

[S1] I. I. Ryabtsev, D. B. Tretyakov, I. I. Beterov, and V. M. Entin, Effect of finite detection efficiency on the observation of the dipole-dipole interaction of a few Rydberg atoms, *Phys. Rev. A* **76**, 012722 (2007); Erratum: *Phys. Rev. A* **76**, 049902(E) (2007).

[S2] J. H. Gurian, P. Cheinet, P. Huillery, A. Fioretti, J. Zhao, P. L. Gould, D. Comparat, and P. Pillet, Observation of a Resonant Four-Body Interaction

in Cold Cesium Rydberg Atoms, *Phys. Rev. Lett.* **108**, 023005 (2012).

[S3] E. A. Yakshina, D. B. Tretyakov, I. I. Beterov, V. M. Entin, C. Andreeva, A. Cinins, A. Markovski, Z. Iftikhar, A. Ekers, and I. I. Ryabtsev, Line shapes and time dynamics of the Förster resonances between two Rydberg atoms in a time-varying electric field, *Phys. Rev. A* **94**, 043417 (2016).

[S4] D. A. Varshalovich, A. N. Moskalev, and V. K. Khersonskii, *Quantum Theory of Angular Momentum* (World Scientific, Singapore, 1988).

[S5] M. Saffman, *Atomic Physics: Structure, Interactions and Entanglement*, 2016 (unpublished).

[S6] S. Weber, C. Tresp, H. Menke, A. Urvoy, O. Firstenberg, H. P. Büchler, and S. Hofferberth, Tutorial: Calculation of Rydberg interaction potentials, *J. Phys. B* **50**, 133001 (2017).

[S7] B. Kaulakys, Consistent analytical approach for the quasiclassical radial dipole matrix elements, *J. Phys. B* **28**, 4963 (1995).